RSC Advances

ROYAL SOCIETY OF CHEMISTRY

www.rsc.org/advances

In vitro gene expression and preliminary *in vivo* studies of temperature-dependent titania–graphene nanocomposites for bone replacement applications

K. Kavitha[1], W. Chunyan[2], D. Navaneethan[1], V. Rajendran[1]*, Suresh Valiyaveettil[2] and A. Vinoth[3]

[1]Centre for Nano Science and Technology, K.S. Rangasamy College of Technology, Tiruchengode – 637 215, Tamil Nadu, India
[2]Department of Chemistry, Faculty of Science, National University of Singapore, Singapore – 117543
[3]Molecular Genetics and Breeding Laboratory, Directorate of poultry Research, Hyderabad- 500 030, India

*Address for correspondence veerajendran@gmail.com

Tel : +91-4288-274741-4

Fax : +91-4288-274880

ABSTRACT

To meet the demand for biomaterials due to increasing bone defects and damages, we sought to synthesize titania–graphene nanocomposites at different sintering temperature and then optimized to explore their potential applications in biomaterials. The nanocomposites with higher surface area (212.85 to 233.87 m^2g^{-1}) and mechanical strength ranging from 0.430 to 2.11 GPa were subjected to 1.5 mM simulated body fluid to confirm their bioactivity mechanisms. Non-significant toxic nature of nanocomposites in MG-63 osteoblast cell lines and controlled swelling and degradation rates indicate the suitability of these materials for biomedical applications. Moreover, the obtained percentage of mitochondrial damage, osteocalcin, Osteopontin and Collagen type - 1 gene expression level in MG-63cell line confirms that the nanocomposite sintered at 400 ºC is more optimal biomimetic material among the prepared nanocomposites. The preliminary *in vivo* toxicity of nanocomposite sintered at 400 ºC in zebrafish (*Danio rerio*) shows non-toxic nature. This optimization studies will help for further research and optimization of promising biomimetic material for the repair and reconstruction of the natural bone tissue.

KEYWORDS: Titania–graphene, *In vitro* cytotoxicity, biocompatibility, Gene expression studies, *In vivo* toxicity, MG–63, zebrafish (*Danio rerio)*

1. Introduction

Graphene, a single atomic layer of graphite with a hexagonal lattice structure, which has drawn intense research interests due to its extraordinary band structure, ultrahigh specific surface area (SSA), and superior electron mobility.[1-3] Especially, the high mechanical property of graphene makes it suitable for biomedical applications through more robust attachment, stimulating the osteointegration and its ability to absorb protein and low-molecular-weight substances.[2-4] On the other hand, titania is an inexpensive and environmentally benign material

that has been widely used in biomedical applications.[5] The presence of Ti–OH constructive site and the occurrence of anatase phase of titania are proficient for deposition of calcium and phosphate, and nucleation of hydroxyapatite (HAp) layer.[6-7] However, there are some issues with the migration and accumulation of titania nanoparticles in cell organelles.[7-9]

Recently, graphene-based metal oxide nanocomposites have drawn more attention due to their synergistic contribution of two or more functional components in many potential applications.[10-12] However, new strategies are required to synthesize and to incorporate graphene-based nanocomposites. Graphene serves as a platform for preparation of composites due to its planar carbon structure and due to the presence of carboxyl and hydroxyl functional groups in its hydrophobic surface, which leads to more robust attachment with the biological materials and improves their aqueous solubility.[3,10] In addition, grapheme is used to induce osteocytes on stem cells and has an osteoconductive/inductive effect, which makes it suitable for bone regeneration therapy.[11,12] Although graphene-based nanomaterials have brought great research interest in biomedical applications, there are still some concerns about the potential toxicity and biocompatibility of these nanocomposites.

In this study, we have experimentally shown the preparation of titania–graphene nanocomposites at different temperature using *in situ* sol–gel method. Furthermore, the prepared samples are analyzed comprehensively to explore their physico-chemical properties. To explore the optimal composite material with properties to promote desired bone tissue regeneration, we studied the biological aspects such as swelling, bioactivity, and biocompatibility, respectively, for phosphate-buffered saline (PBS), simulated body fluid (SBF), and osteoblast-like cell lines (MG-63) of the prepared nanocomposites. In addition, gene expression and their quantification in

nanocomposite-treated MG-63 cell line and preliminary *in vivo* toxicity analysis in zebrafish were carried out to explore their optimal properties for bone cell regeneration.

2. Materials and methods

2.1. Nanocomposite preparation

Graphene oxide was synthesized using Hummers method from graphite flakes, as reported earlier.[13-15] Graphite flakes (Catalog No.: 332461, Sigma–Aldrich, USA, 98%) and sodium nitrate ($NaNO_3$, CAS No.: RM1722, HiMedia, 99%99%; HiMedia) were added into a round-bottom flask and stirred in ice bath at a ratio of 2:1 (w/w). A mixture of 44.2% (v) of concentrated sulfuric acid (H_2SO_4, CAS No.: 7664-93-9, Merck, 98.08%) and 4.6% (w) potassium permanganate ($KMnO_4$, CAS No.: 7722-64-7, Merck, 99%) was added slowly for 1 h. After oxidation, a homogeneous solution was obtained. Then, the solution was kept at room temperature and stirred for another 1 h. Following the above procedure, 30% of hydrogen peroxide (H_2O_2, CAS No.: 7722-84-1, Merck, 30%) solution was added to convert graphite into graphite oxide. To remove the impurities from the obtained thick solution, ultrapure water was added and then it was centrifuged repeatedly. Then, the mixture was dried initially at 80 °C and then sintered at 300 °C to form the graphene oxide. The obtained graphene oxide was converted to graphene by using the hydrazine hydrate (N_2H_5OH, CAS No.: 7803-57-8, Loba Chemie, 80%).[13-16] Then, the prepared graphene was dispersed in ultrapure water under sonication and was used for the preparation of titania–graphene nanocomposite.

Analytical grade titanium isopropoxide (($Ti(OC_3H_7)_4$, Catalog No.: 205273, Sigma–Aldrich, USA, 97%) was diluted in isopropyl alcohol ($CH_3CHOHCH_3$, CAS No.: 67-63-0, Merck, 99.7%), acetyl) with hydrolysis controller acetyl acetone ($C_5H_8O_2$, CAS No.: 123-54-6, Loba Chemie, 98.4%) in the molar ratio of 1:0.7:4.[7] According to our previous study,[17] the

optimized ratio of graphene and titania (1:1) were used in this study for further optimization of nanocomposites with different parameter. The dispersed graphene was drop-wise added to titanium mixture under sonication for 1 h. Then, the sonicated solution was stirred continuously for 4 h at 310 K. The obtained precipitate was washed with double-distilled water followed by washing with ethanol using centrifugation and then dried in a hot-air oven at 180 ºC to evaporate the solvents. Then, the obtained dried powder was termed as TG. The TG samples were sintered at 400 and 600 ºC for 1 h (hereafter termed as TG-400 and TG-600, respectively). The prepared nanocomposites (TG, TG-400, and TG-600) were well ground using mortar and pestle and then stored in desiccators to avoid agglomeration.

2.2. Characterization

The crystalline nature of the prepared nanocomposites was studied using X-ray diffractometer (XRD) (X'Pert PRO; PANalytical, the Netherlands) with Cu Kα as the radiation source (λ = 0.15406 Å). Scherrer formula was used to obtain X-ray spectral peaks to determine the average crystal size of the nanocomposites.[18] The occurrences of the composite of graphene and TiO_2 are analysised through the Raman spectra (RENISHAW– M005–141) with the laser frequency of 514 nm. X-ray fluorescence (XRF) spectrometry (EDX-720; Shimadzu, Japan) and scanning electron microscopy with energy-dispersive X-ray spectroscopy (SEM–EDX) (JSM-6390LV; JEOL, Japan) techniques were used to analyze the elemental composition both qualitatively and quantitatively along with surface morphology of the prepared nanocomposites. The primary particle size was estimated using transmission electron microscopy (TEM) (CM200, Philips, USA). The SSA of the prepared nanoparticles was measured using the Brunauer–Emmett–Teller analyzer (Autosorb AS-1MP; Quantachrome, USA). The total pore volume and the average pore diameter of the prepared nanocomposites were measured from the SSA of the

samples using the Brunauer–Joyner–Halenda method.[19] The mechanical properties, namely, nanohardness (*H*) and Young's modulus (*E*), of the nanocomposite were evaluated by a mechanical testing machine (Ubi 1 Scanning Quasistatic Nanoindentation (TI-700); Hysitron, USA) by keeping the loading and unloading time as constant as 5 s at a rate of 200 nm s^{-1}.

2.3. Swelling and degradation analyses

The swelling and degradation behaviors of the prepared samples were analyzed in PBS (pH 7.4 at 37±1 ºC) and 10,000 μ mL^{-1} lysozyme-containing PBS for 1 and 3 weeks.[7,20,21] The prepared samples were made into pellets using a hydraulic pressure pellet maker. Three pellets in each prepared sample (TG, TG-400, and TG-600) were incubated in PBS and lysozyme-containing PBS for different periods. The incubated pellets were removed from the solutions on 1, 4, and 7 days for swelling study and 1, 2, and 3 weeks for degradation study. The removed pellets were washed with ultrapure water. The wet weight and dry weight of the samples were measured after removing the surface-adsorbed water and then compared with the initial weight of nanoparticles. The swelling and degradation percentages were calculated by the following formulas.[20,21]

$$\text{Percentage of swelling} \quad W_G(\%) = \frac{W_w - W_0}{W_0} \times 100 \qquad (1)$$

$$\text{Percentage of degradation } W_L(\%) = \frac{W_0 - W_t}{W_0} \times 100 \qquad (2)$$

where W_0 is the initial weight of the pellets, W_w the wet weight of the pellets after swelling study, and W_t the dry weight of the pellets after the degradation study.

2.4. In vitro bioactivity study

The prepared nanocomposite samples (TG, TG-400, and TG-600) were analyzed in 1.5 SBF to check the bioactive capability, that is, the formation of bone-like apatite layer on the

surface of the samples. The standard procedure[22,23] was used to prepare the 1.5 SBF *in vitro* levels having a similar environment of *in vivo* with the analytical grade of sodium chloride (Merck, 99.5%), sodium hydrogen carbonate (Loba Chemie, 99.5%), potassium chloride (Merck, 99.5%), di–potassium hydrogen phosphate trihydrate (Merck, 99%), magnesium chloride hexahydrate (Merck, 98%), calcium chloride (Merck, 99.5%), sodium sulfate (Merck, 99.5%), Tris–hydroxymethyl aminomethane (Tris, Loba Chemie, 99.5%) and 1M (mol/l) or 67.5 mM hydrochloric acid (Loba Chemie, 35-38%) were used.[22-24] Preweighted pellets (W_0) were immersed in 1.5 SBF and then incubated for 21 days at 37±1 ºC in a circulating water bath. The pH and conductivity probes of 5-Star (Thermo Orion, USA) were regularly used to record the ion exchange between the SBF and the prepared sample. After incubation, the weight loss was calculated using the following formula with wet weight of the pellets (W_w)

$$\text{Weight loss ratio } W_L\ (\%) \ : \frac{W_w - W_0}{W_0} \times 100 \qquad (3)$$

The formation of HAp layer on the surface of the pellets was analyzed using XRD and XRF methods.

2.5. Cell line studies

MG-63 osteoblast cell line was used to study the biocompatibility and bone-forming ability of the material.[24] The cell lines were passed through RPMI-1640 medium (catalog no. R8758) containing 10% fetal bovine serum, nonessential amino acids, 100 µg mL^{-1} penicillin, and 100 µg mL^{-1} streptomycin at 37±2 ºC with 5% CO_2. The mitochondrial damage of the prepared nanocomposite-treated MG-63 cells was estimated using 3-(4,5-dimethylthiazol-2-yl)-2,5-diphenyltetrazolium bromide (MTT, catalog no. 070M61471) kit assay.[7,24] A total of 1×10^3 confluent cells were seeded into a microtitrate plate and then allowed to incubate for 24 h to

adhere them on the plate. Then, the filter-sterilized nanocomposites (TG, TG-400, and TG-600) MTT solution dimethyl sulfoxide (DMSO) was loaded one by one at a defined incubation period to titer the toxicity of the samples. Then, the optical density (OD) of the assay was observed at 570 nm. The percentage of cell viability was calculated using the following formula:

$$\text{Percentage of cell viability} = \frac{\text{OD of the nanoparticle-treated cells}}{\text{OD of the control cells}} \times 100 \quad (4)$$

2.6. Osteocalcin estimation

Osteocalcin (OCN) is a bone γ-carboxyglutamic acid containing protein and abundant Ca^{2+}-binding protein primarily deposited in the extracellular matrix of bone. This non-collagenous protein plays a curial role in bone mineralization and calcium ion homeostasis (regulation of bone mass), energy metabolism and fertility. The bone growth is directly depends on the presence of osteocalcin in EMC.[25] The estimation of OCN production in nanoparticle-treated osteoblast-like MG-63 cell line helps us explore the effect of nanocomposites on bone induction.[24] Highly specific monoclonal antibodies and peroxidase-labeled osteocalcin containing ELISA kit (Biological Technologies, Inc., USA) were used to estimate the level of osetocalcin. The level of OCN protein in cell culture supernatants was measured after a period of 21 days of incubation by absorbance at 450 nm wavelength, and it was expressed μg^{-1} ng. Cells grown in the absence of prepared nanocomposites served as a control.

2.7. Gene expression analysis using real-time PCR

2.7.1. RNA extraction and cDNA Synthesis

Total RNA was extracted from the prepared nanocomposites treated MG-63 cell line using TRIzol reagent (Invitrogen, USA) and standard protocols.[26, 27] The purity of the RNA was assessed by absorbance at 260/280 nm ratio (Genova Nano Micro - Volume spectrophotometer,

UK). First strand cDNA was synthesized from obtained 1.5 µg of total RNA samples using an Oligo dT primer and reverse transcriptase according to the manufacturer's protocol (Applied biosystem, USA).

2.7.2. Quantitative real-time RT-PCR

To monitor the new bone synthesis, specific marker genes such as of osteopontin (OPN), osteocalcin (OCN) and collagen type I (COL 1), and beta actin mRNA transcripts as a endogenous control are quantified using real-time PCR. The forward and reverse primers which used for the RT-PCR are synthesized using NCBI –BLAST and Primer plex (Applied biosystem, UK). The primer sequences are shown in Table 3. The reactions were prepared with duplicate in a final volume of 25 µl, comprised of 12.5 µl Power SYBR® Green PCR Master mix (Applied biosystem, UK), 2 µl each of forward and reverse primer (µM), 6.5 µl of distilled H_2O and 2 µl of cDNA. The amplification protocol was followed as: initial denaturation at 95°C for 10 min, followed by 40 cycles of cyclic denaturation at 94°C for 15 s, annealing at 58°C for 1 min and a final extension at 72°C for 15 s. Real-time PCR reactions were carried out by Mx-3000P thermocycler (Stratagene, USA). The whole experiment was repeated as triplicates and the data were expressed as fold change compared with control and standard formula used in the previous studies.[26,27]

2.8. Preliminary in vivo experiment in zebrafish

Healthy wild-type zebrafish (*Danio rerio*) embryos with eight-cell stage (4–16 cell stage) were selected and maintained at a temperature of 27±2 °C and a pH of 6.5–7. According to a well-established procedure[28] the embryos were treated with 100 mg mL^{-1} concentrations of each prepared nanoparticle and then incubated for a specific period (48 and 72 h) to explore the effect on embryonic development. The preliminary morphological changes such as mortality

rate, hatching rate, growth retardation, touch responses, and edema accumulation were monitored.

2.9. Statistical analysis

Statistical Package for the Social Sciences software (version 16.0, SPSS Inc., USA) was used to analyze the significance of the obtained *in vitro* results. The triplicate results of cell line studies were typically represented as an arithmetic mean and standard deviation. Tukey's least-significant difference and Duncan's *post hoc* tests were used to explore the statistical significance. For gene expression studies, two way Annova was used. Statistical significance was considered at 5% level and then compared with the untreated MG-63 cell line.

3. Result and discussion

3.1. Properties of the nanocomposites

The crystalline phase of prepared nanocomposites is shown in XRD pattern (Fig. 1). As indicated in Fig. 1a, the obtained broad diffraction peaks at 25.28° (hkl = 101, JCPDS file no.: 21-1272) and 25.35° ((hkl = 101, JCPDS file no.: 894921) are responsible for the titania tetragonal anatase phase with body centred lattice arrangements. In addition, the observed high intensity peak at 26.6° (JCPDS file no. 411487) confirm the presence of graphene with the crystalline titania.[13,29-32] The other observed intensity peaks (Fig. 1) at 37.8 (004), 38.5 (112), 48.0 (200), 53.9 (105), 55.1 (211), 62.68 (204), 68.82 (116) and 75.02 (215) corresponds to the anatase phase of titania (JCPDS file no. 21-1272 & 894921). However, the increase in sintering temperature of titania–graphene nanocomposites increases the low-intensity small hump at 12.7^{o}, which is responsible for the trace amount of graphite oxide.[30,31] This may be due to reconversion of graphene oxide from the unfound graphene. The average crystallite size obtained using Scherrer equation[26] and is given in Table 1. In our previous study,[17] the addition of

nanographene into the nanotitania showed a decrease in crystallite size and crystalline nature. Furthermore, this study reveals an increase in sintering temperature of titania–graphene nanocomposite accompanied by an increase in crystallite size. This is probably due to the dominant effect of temperature on nucleation process.[31]

TEM images of all prepared samples are shown in Fig. 2. It shows the particle size of the nanocomposites with an average diameter of 20 nm. Similar to crystallite size, the particle size also increases with an increase in the sintering temperature.[32-34] The primary particle size of the prepared TG is 8.21 nm, although after sintering the TG at 400 and 600 °C the particle size is increased to 8.19 and 8.86 nm, respectively. The observed results confirm that the sintering temperature plays a role in determination of the particle size and agglomeration of the finer particles (Fig. 2).[33] The selected area electron diffraction (SAED) pattern of the nanocomposites is inserted into their respective TEM images. The SAED is well indexed with the XRD pattern and confirms that the increase in sintering temperature increases the crystalline nature of titania–graphene nanocomposites. SEM result shows sheet-like morphology, which reveals the presence of spherical titania balls embedded onto the graphene sheets (Fig. 3). In addition, the elemental compositions of prepared samples are shown in Fig. 3 (EDX). The reduction of carbon content in the nanocomposites is reciprocal to an increase in temperature of the nanocomposite; this is in line with the earlier studies.[33,34]

Similar to earlier studies,[32-34] we observed that the increase in sintering temperature increases the SSA of the prepared nanoparticle, that is, the SSA of the prepared TG was 212.85 m^2g^{-1}, while sintering the TG nanocomposites a gradual increase in the SSA was observed as 216.04 and 233.87 m^2g^{-1} for TG-400 and TG-600, respectively (Fig.4). The obtained mesoporous surface area favors the cell attachment and three-dimensional cell growth during the

implantation and tissue engineering.[7,34] Similarly, mechanical strength is essential for the biomaterials to withstand in the human body until new bone is grown.[4,35] The mechanical strength of the prepared nanocomposite TG is 0.430 GPa, whereas the sintered nanocomposites (TG-400 and TG-600) show an increased mechanical strength of 1.46 and 2.11 GPa, respectively. An increased mechanical strength is due to crystalline arrangements of the material and its moisture-free nature.[35,36]

The Raman spectroscopic analysis of prepared TiO_2-graphene nanocomposites is shown in Fig.5. The presence of TiO_2 is revealed from the bands observed at 148, 396, 519 and 639 cm^{-1}.[37] Specifically, the bands observed at 148 and 396 cm^{-1} are responsible for the presence of anatase and 519 and 639 cm^{-1} for rutile. The obtained Raman spectrum indicates that the intensity of anatase TiO_2 bands is decreased while increasing the sintering temperature of the nanocomposites. This observation indicates the anatase phase of TiO_2 is slightly starts to convert as a rutile phase.[38] decreases with the increase in the concentration of graphene Moreover, this non-destructive analysis shows the presence of G and D bands of graphene at ~1588 and 1355 cm^{-1} along with the 2D peak at ~2650 cm^{-1}.[16,37,39]. The intensity of the G and D bands decreases with the increase in the sintering temperature, which confirms the reconversion of graphene to graphite slightly. This is further supported by formation of 2D peaks at the higher sintering temperature of the nanocomposites. The obtained Raman spectra confirm the existence of graphene and the formation of TiO_2-graphene nanocomposites. This is in line with the obtained FTIR results and previous Raman reports.[37,39,40]

3.2. In vitro analysis

3.2.1. Swelling and degradation behavior

The obtained swelling and degradation percentages of nanocomposites are given in Table 2. Swelling tendency of the particles depends on various parameters such as the presence of ions, material property, and temperature.[7-22] An abundant swelling was observed in PBS than in water, which is due to the presence of ions in the solution. However, notable swelling and degradation properties were observed in both PBS and ultrapure water, which is due to the material's property.[19-20] Graphene surface has an ability to absorb protein and low-molecular-weight substances including bone morphogenetic protein, which is due to the creation of the benzene ring by van der Waals forces.[17,36] Nanocomposites prepared at 400 °C (TG-400) attain a maximum swelling property in PBS (24.65%) and water (20.89%). Similarly, TG-400 attains maximum degradability in PBS (21.65%) and water (19.65%). As like obtained SSA, mechanical strength, and swelling and degradation properties also depend on the sintering temperature of the material for the optimal ability. Consequently, it is assumed that the above parameters may play a dominant role in the bioactivity, osteogenic differentiation, and proliferation through adequate interaction with the biological environment.[7]

3.2.2. Bioactivity study

The obtained significant changes in pH and conductivity of 1.5 SBF-immersed nanocomposites (TG, TG-400, and TG-600) are shown in Fig. 6. The ionic interaction pattern of TG sample (during the 21 days of incubation) is similar to that of samples TG-400 and TG-600. However, TG-400 shows higher crest and trough among the prepared nanocomposites. Up to the 18th day of incubation, crest and trough values are obtained in both pH and conductivity studies. The results confirm the exchange of ions between the composites and SBF due to formation of HAp layer on the surface of the samples. On the 18th day, the pH and conductivity show a stable phase, which is due to saturation of the supplementary ions to initiate the formation of HAp layer

on the surface (Fig. 6a and 6b).[7,17] The observed ion exchange measurements reveal that the prepared TG-400 sample is more vibrant to interact with human tissues than TG and TG-600.

After carrying out the 1.5 SBF study, the nanocomposites were subjected to an XRD study to confirm the existence of their bioactivity (HAp layer formation). Fig. 1b shows a distinct diffraction peak at 31.7° (211), 45.3 (203), 46.7 (222) and 49.4 (213), which indicates the presence of crystalline HAp layer (JCPDS file no. 090432 and 721243). The obtainted peaks at 45.3 degree are slightly different loacation in prepared nanocomposites. The TG and TG-600 shows the peak at 45.3 degree (hkl=203, hkl-f= 6, 36). Similarly in TG-400, the peak is obtained at 46.7 (hkl=222, hkl-f =30, 267). Both the peaks represent the formation of HAp layer as per the above JCPDS files. Moreover, the observed high intensity peak at 25.35 (Fig. 1b) is due to the domination of TiO_2. Therefore, the observed results confirms that the observed peak at 25.35 is corresponds to TiO_2 phase and also HAp peak intensity is predominant at 32^{o}, which is clearly shown in Fig 1b. A dramatic increase in crystallite size (Table 2) is observed when the nanocomposites is immersed in SBF, which is associated with the agglomeration of nanoparticles in biofluid (SBF) and the formation of HAp layer.[32,36] When compared with the prepared TG, both the sintered composites (TG-400 and TG-600) reveal an increase in the intensity of HAp crystalline peaks and a peak shift toward the lower wavelength side. XRD patterns (before and after bioactivity study) of the prepared samples (Fig.1a and 1b) show that TG-400 has well-formed crystalline peaks. It reveals nanocomposites prepared at 400 °C is the optimal temperature for arrangements of TiO_2 lattice on the basal plan of the graphene, which is further supported by the obtained particle size, crystallite size, surface area, swelling, and biodegradability.[13,41]

The weight modulation after *in vitro* SBF study confirms that an increase in sintering temperature increases the weight loss of the nanocomposites (Table 2). Similarly, the measured quantity of calcium and phosphate depositions on the sample observed through the XRF study is given in Table 2 along with the Ca/P ratio obtained by comparing the initial weight of calcium and phosphate of the samples. The obtained stoichiometric Ca/P ratio of the prepared TG (1.58) and TG-400 (1.63) nanocomposites is in the range of formation of oxy-HAp (1.5 to 1.67), while that of the TG-600 (1.75) shows the formation of carbonate-substituted HAp.[7,17,42] The above observation confirms that the titania–graphene nanocomposite sintered at 400 °C with a stoichiometric Ca/P ratio of 1.63 is the most favorable material for the bone repair and regeneration, which is evident from the observed results (physicochemical, swelling, and degradability properties). The sintering temperature above and below 400 °C confers the carbonate-substituted HAp or calcium-deficient HAp, rather than the appropriate bone-like oxy layer. Further, to confirm the HAp formation with calcium phosphate deposition on the surface of the sample, SEM image with EDX pattern after carrying out the 1.5 SBF study is included in Fig.7. The surface morphology indicates that the deposition of Ca and P on surface of the nanocomposites[43] which is further clearly confirmed through the EDX pattern. The observed results are in good agreement with the obtained XRF result.

3.2.3. Biocompatibility with osteocalcin analysis

Graphene as a composite has the ability to accelerate osteogenic differentiation of human mesenchymal stem cells and pluripotent stem cells.[11,12] Fig. 8 shows the MTT assay of osteoblast-like MG-63 cell lines, which are exposed to prepared titania–graphene nanocomposites at different concentrations (1, 5, and 20 μg mL^{-1}). The SPSS analysis shows non-significant toxicity ($p < 0.05$) of the above sample with control MG-63 cell lines. Moreover,

little toxicity at the higher and lower sintering temperature is observed, which may be due to crystalline alignment. Similarly, concentration-dependent mitochondrial damages are also observed in Fig. 8. The above observations confirm that the parameters such as type of precursor, dosage, and synthesis procedure play a major role in determining the biocompatibility of the material. Moreover, temperature is also one of the key parameters in the analysis of toxicity.

Osteocalcin is a bone γ-carboxyglutamic acid-containing, noncollagenous, multifunctional protein found abundantly in extracellular matrix of the bone. It regulates bone mineralization, calcium ion homeostasis, insulin, energy expenditure and fertility.[24,25,28,30] The obtained OCN estimation in all the three nanocomposites confirms that an increase in the sintering temperature leads to an increase in the production of OCN (Table 2); it may be due to the optimal lattice arrangements of nano TiO_2 on the basal and egde plane of graphene their ability to interact with the cell induction and bone mineralisation process.[13,42] It is clear from Table 2 that the prepared TG shows a lower secretion of OCN protein when compared to that of sintered nanocomposites. Both the sintered nanocomposites (TG-400 and TG-600) during all the incubation periods reveal a similar secretion of OCN. This is evident from the observed homogenous subsets of non-significant difference at $p < 0.05$ (Table 2), although at the end of 21st day of incubation, TG-400 shows a higher secretion of OCN in a customary way.

3.2.4.Gene expression analysis

The gene expression datas are presented as mean (n = 3). The obtained OSC, OPN and COL 1 data are statistical compared and represented in Fig. 9. The relative expression of the all genes are normalised against a housekeeping gene (β-actin). In line with the previous reports of titanium, graphene, bioceramics,[26,27,44,45] the obtained result shows that the up-regulation in the production of bone related proteins like OCN, OPN and COL 1 collectively (Fig. 9). This is

inturn to supports the new bone formation. Compare with the OPN expression, the expressions of OCN and then the COL 1 are relatively higher. Especially OCN shows significant difference at $p<0.05$ than the COL 1 (Fig. 9). Eventhough the obtained result shows imprecise in optimisation of sintering temperature, TG-400 sample shows good fold up-regulation (2.28 fold = OCN, 1.23 fold = OPN and 1.23 fold = COL 1 up regulation) with $p<0.05$ statistically significance. This result supports the above physico-chemical parameters and its influences.

3.3. Effect of nanoparticles on the zebrafish

The preliminary *in vivo* toxicity study was repeated thrice and average mean values were recorded and are given in Table 4. The optimized titania–graphene nanocomposite from the *in vitro* studies is used to analyze the preliminary level of *in vivo* cytocompatibility employing the easily available zebrafish embryos. The nanocomposite-unexposed zebrafish embryos are taken as control and compared with the TG-400 nanocomposite-exposed embryos. These embryos show a nonsignificant mortality rate, which is proved statistically (Table 4). However, TG-400 nanocomposite-exposed zebrafish after 48 h show an increase of 30% (20% normal + 10% upnormal) in the hatching rate compared to the controls (Fig. 10). On the other hand, after the 72 h of exposure, TG-400 nanocomposite-exposed zebrafish show nonsignificant mortality and upnormality rate when compared with the controls. In recent years, zebrafish is widely used as an inexpensive and good *in vivo* model to check toxicity.[46,47] Previous studies show the 100 μg mL^{-1} dosage of silver and silver nanoparticles causes the toxicity to zebrafish by observing severe oedema and respiratory blocking.[46] Similarly, the liver and intestine of the rainbow trout are affected mostly by the dosage of 0.1 mg L^{-1} TiO_2, whereas at higher dosage (1.0 mg L^{-1}) it affects gills and brain of the rainbow trout.[47] The above preliminary result confirms that the prepared titania–graphene nanocomposite sintered at 400°C (TG-400) is not toxic in zebrafish.

4. Conclusions

The titania–graphene nanocomposite was prepared by *in situ* sol–gel method and treated at 400 and 600 °C. The base nanocomposite (TG) was compared with the sintered nanocomposites (TG-400 and TG-600) in terms of physico-chemical and *in vitro* analyses. The crystalline nature, particle size (8.11–8.86 nm), crystallite size (3.01–3.23 nm), and OC production of the sintered nanocomposites (TG-400 and TG-600) were found to increase with the increase in sintering temperature of the TG. However, the SSA (233.87 m^2g^{-1}), mechanical strength (1.46 GPa), and swelling (25.55%) and degradation tendency (121.68%) of the sintered nanocomposites at 400 °C reveal that TG-400 is a more optimal composite than TG and TG-600 nanocomposites due to the better lattice arrangements. In addition, the results obtained from bioactivity study (Ca/P ratio) and cytotoxicity assay in MG-63 support the above statement. Moreover, the gene expression studies support the new bone synthesis via up regulated bone specific markers, especially TG-400 sample with OCN production. The present study was aimed as a preliminary *in vivo* screening of *in vitro* optimised nanocomposites such as morphological changes, growth retardation, and hatching and mortality rates of the zebrafish embryos. This study robustly confirms that TG-400 is potential nanocomposites for further molecular level *in vivo* analysis which will help to found more appropriate nanocomposite for the current requirements of bone repair and regeneration among the prepared nanocomposites.

ACKNOWLEDGMENTS

This work was supported by UGC–DAE–Consortium for Scientific Research, Kalpakkam (CSR/Acctts/2010–11/1136 dt.06.01.2011). The authors thank Dr. G. Amarendra (Head, Metal Physics Section, Indira Gandhi Centre for Atomic Research, Kalpakkam node) for constructive suggestions.

REFERENCES

1. M. J. Li, C. M. Liu, Y. B. Xie, H. B. Cao, H. Zhao and Y. Zhang, *Carbon,* 2014, **66**, 302 –311.
2. S. Ryu and B. S. Kim, *Tissue Eng. Regen. Med*., 2013, **10**, 39–46.
3. H. Zhang, G. Gruner and Y. Zhao, *J. Mater. Chem. B*, 2013, DOI: 10.1039/c3tb20405g.
4. C. Zhu, S. Guo, P. Wang, L. Xing, Y. Fang and Y. Zhai, *Chem. Commun.,* 2010, **46**, 7148–7150.
5. Y. I. Jhon, Y. M. Jhon, G. Y. Yeom and M. S. Jhon, *Carbon*, 2014, **66**, 619–628.
6. D. Hua, K. Cheuk, Z. Wei–ning, W. Chen, X. Chang–fa, *Trans. Nonferrous. Met. Soc. China*, 2007, **17**, 700–703.
7. K. Kavitha, S. Sutha, M. Prabhu, V. Rajendran and T. Jayakuma, *Carbohydr. Polym.* 2013, **93**, 731–739.
8. A. Kroll, C. Dierker, C. Rommel, D. Hahn, W. Wohlleben, C. Schulze–Isfort, *Part Fibre. Toxicol*. 2011, **8**, 9.
9. S. Singh, T. Shi, R. Duffin, C. Albrecht, D. V. Berlo and D. Hohr, *Toxicol. Appl. Pharmacol.,* 2007, **222**, 141-151.
10. X. Zhang, Y. Sun, X. Cui, S. A. Jiang, *Int. J. Hydrogen Energy*, 2012, **37**, 811–815.
11. H. Chen, M. B. Muller, K.J. Gilmore, G.G. Wallace, D. Li, *Adv. Mater*., 2008, **20**, 3557–3561.
12. T. R. Nayak, H. Andersen, V.S. Makam, *ACS Nano*., 2011, **5**, 4670–4678.
13. X. Y. Zhang, H.P. Li, X.L. Cui, Y. Lin, *J. Mater. Chem*., 2010, **20**, 2801–2806.
14. S. Stankovich, D. A. Dikin, R. D. Piner, K. A. Kohlhaas, A. Kleinhammes, Y. Jia, *Carbon*, 2007, **45**, 1558–1565.

15. Y. Liang, H. Wang, H.S. Casalongue, Z. Chen, H. Dai, *Nano Res*., (automatically inserted by the publisher).

16. M. Selvam, K. Sakthipandi, R. Suriyaprabha, K. Saminathan, V. Rajendran, *Bull Mater Sci*. 2013, **36**, 4.

17. K. Kavitha, M. Prabhu, M. Selvam, V. Rajendran, *Mat. Sci. Engine. C*, 2014, **48**, 252-262.

18. N. Duraisamy, N. M. Muhammad, H. C. Kim, J. D. Jo, K. H. Choi, *Thin Solid Film,*. 2012, **520**, 5070–5074.

19. E. P. Barrett, L. G. Joyner, P. P. Halenda, *J. Am. Ceram. Soc*. 1951, **73**, 373–380.

20. V. V. D. Rani, R. Ramachandran, K. P. Chennazhi, H. Tamura, S. V. Nair, R. Jayakumar, *Carbohydr. Polym*., 2011, **83**, 858–864.

21. Y. Huang, M. Seng, J. Ren, J. Wang, L. Fan, Q. Xu, *Colloids Surf. A: Physicochem. Eng. Aspects*, 2012, **401**, 97–106.

22. L. Radev, K. Hristova, V. Jordanov, M. H. V. Fernandas, I. M. M. Salvado, *Cent. Eur. J. Chem.,* 2012, **10**, 137–145.

23. L. C. Gerhardt, G. M. R. Jell, A. R. Boccaccini, *J. Mater. Sci. Mater. Med*., 2007, **18**, 1287–1298.

24. R. Kue, A. Sohrabi, D. Nagle, C. Frondoza, D. Hungerford, *Biomaterials*, 1999, **20**, 1195–1201.

25. C. Kasperk, J. Wergedal, D. Strong, J. Farley, K. Wangerin, H. Gropp, *J. Clin. Endocrinol. Metab.,* 1995, **80**, 8, 11–7.

26. S. W. Tsai, H. M. Liou, C. J. Lin, K. L. Kuo, Y. S. Hung, R. C. Weng, F. Y. Hsu, *PLoS ONE,* 2012, **7(2),** e31200.

27. S. Heinemann, C. Heinemann, M. Jeager, J. Neunzehn, H. P. Wiesmann, and T. Hanke, ACS Appl. Mater. Interfaces 2011, 3, 4323–4331.

28. P. V. Asharani, Y. Lianwu, Z. Gong, S. Valiyaveettil, *Nanotoxicol*. 2011, **5**, 43–54.

29. H. C. Kim, N. Duraisamy, N. M. Muhammad, I. Kim, H. Choi, J. Jo, J. *Appl. Phys. A*, 2012, **107**, 715–722.

30. K. Krishnamoorthy, G. S. Kim, S. J. Kim, *Ultrason. Sonochem*., 2013, **20**, 644–649.

31. K. Krishnamoorthy, M. Veerapandian, L. H. Zhang, K. Yun, S. J. Kim, *J. Phys. Chem. C*, 2012, **116**, 17280–17287.

32. K. Kavitha, M. Prabhu, V. Rajendran, P. Manivasankan, P. Prabu, T. Jayakumar, *Curr. Nanosci.,* 2013, **9**, 308-317.

33. P. Manivasakan, V. Rajendran, P. R. Rauta, B. B. Sahu, P. Sahu, B. K. Panda, S. V. Veetil, & S. Jegadesan, *J. Am. Ceram. Soc*.. 2010, **93**, 2236–2243.

34. P. Manivasakan, V. Rajendran, *J. Am. Ceram. Soc*., 2011, **94**, 1410–1420.

35. Q. Xu, H. Fan, Y. Guo, Y. Cao, *Mat. Sci. Engine. A*, 2006, **435**, 158–162.

36. X. Ma, Y. Li, W. Wang, Q. Ji, Y. Xia, *Eur Polym J*. 2013, **49**, 389–396.

37. X. Zhang, Y. Sun, X. Cui, Z. Jiang, , *Int J Hydrogen Energy*, 2012, **37**, 811-815.

38. D. Fang, K. Huang, S. Liu, J. Huang, *J. Braz. Chem. Soc.*, 2008, **19**, 1059-1064.

39. O. Akhavan, E. Ghaderi, *ACS Nano*, 2010, **4 (10),** 5731-5736.

40. J. B. Condon, *British Library Cataloguing in Publication Data*, 2006, USA.

41. M. Z. B. Hussein, M. A. Yarmo, M. Z. H. A. Rahman, Z. Zaina, A. A. S. Liang, *Malaysian J. Analy. Sci*., 2001, **7**, 35-40.

42. K. Kavitha, S. Sutha, M. Prabhu, V. Rajendran, T. Jayakumar, *Carbohydr. Polym,* 2013, **93**, 731-739.

43. S. Sutha, K. Kavitha, G. Karunakaran, V. Rajendran. *Matr. Sci. Eng. C,* 2013, **33**, 4046–4054

44. Y. Xie, H. Li, C. Zhang, X. Gu, X. Zheng, L. Huang, *Biomed. Mater.,* 2014**, 9,** 025009 (7pp).

45. A. Pozio, A. Palmieri, A. Girardi, F. Cura, F. Carinci*, Dent Res J.,* 2012, **9 (8)**, S164-8.

46. K. Bilberg, M. B. Hovgaard, F. Besenbacher, E. Baatrup, *J. Toxicol.,* 2011, **2012**, 9.

47. G. Federici, B. J. Shaw, R. D. Handy. *Aquatic. Toxicol.,* 2007, **84**, 415–430.

CAPTION FOR FIGURES

Fig. 1 X–ray diffraction pattern of a series of titania–graphene nanocomposite for bioactivity a) Before *in vitro* bioactivity study b) After *in vitro* bioactivity study

Fig. 2 Transmission electron microscopic images and corresponding diffraction pattern of prepared titania–graphene nanocomposites a) TG, b) TG-400 and c) TG-600

Fig. 3 Scanning electron microscopic images with respective EDX pattern of titania–graphene nanocomposites a) TG, b) TG-400 and c) TG-600

Fig. 4 BET surface area of titania–graphene nanocomposites

Fig. 5 Raman spectra of titania–graphene nanocomposites

Fig. 6 Measurmements of ionic exchanges between 1.5 SBF and titania–graphene nanocomposites a) pH versus soaking period b) Conductivity during i*n vitro* bioactivity

Fig. 7 SEM images with respective EDX pattern of titania–graphene nanocomposites after SBF bioactivity study a) TG, b) TG-400 and c) TG-600

Fig. 8 Dose dependent viability of MG–63 cells incubated with different concentrations of prepared titania–graphene nanocomposites using MTT assay

Fig. 9 Gene expression studies of TG nanocomposite treated MG–63 cell line. (*) represents significant difference at $p < 0.05$

Fig. 10 Preliminary *in vivo* analysis of titania–graphene nanocomposite in zebrafish a) control and b) TG-400

TABLES

Table 1 Physico–chemical, swelling and degradation properties of prepared titania–graphene nanocomposites

Sample name	Crystallite size (nm)	Particle size (nm)	Mechanical test		Swelling Percentage		Degradation Percentage	
			H (GPa)	E (MPa)	PBS (%)	Water (%)	PBS (%)	Water (%)
TG	3.01	8.11	0.43	82.79	25.55	20.16	20.25	16.15
TG–400	3.13	8.19	1.46	111.82	24.65	20.89	21.68	19.65
TG–600	3.23	8.86	2.11	330.56	22.13	19.23	20.54	14.54

Table 2 *In vitro* bioactivity and osteocalcin content of titania –graphene nanocomposites

Sample name	After *in vitro* SBF study			Osteocalcin content			
	Ca/P ratio (%)	Weight modulation (%)	Crystallite size (nm)	1 ($\mu g^{-1}ng$)	7 ($\mu g^{-1}ng$)	14 ($\mu g^{-1}ng$)	21 ($\mu g^{-1}ng$)
TG	1.58	0.89±0.10	28.74	9.50 ± 0.3^{bc}	9.68 ± 0.5^{bc}	10.67 ± 0.6^{bc}	10.25 ± 1.0^{bc}
TG–400	1.63	1.09±0.2	34.47	10.27 ± 1.3^{bc}	15.22 ± 1.0^{a}	14.43 ± 1.2^{ab}	14.40 ± 1.5^{ab}
TG–600	1.75	1.12±0.21	37.74	11.27 ± 0.3^{bc}	14.55 ± 1.3^{a}	15.88 ± 1.5^{a}	13.32 ± 1.5^{ab}

$^{a,\ ab}$ and ^{bc} represents homogenous subsets of non– significant difference at $p < 0.05$

Table 3 Design of primers for the RT-PCR

Gene	Forward Primer (5'to 3')	Reverse Primer (5'to 3')
OCN	CTGTGACGAGTTGGCTGAC	CTGTGACGAGTTGGCTGAC
OPN	AAGCGAGGAGTTGAATGGT	TTCAGCACTCTGGTCATCC
COL-1	CCACCAATCACCTGCGTACA	GCAGTTCTTGGTCTCGTCACA
β-actin	ACGGGTTCTGGGTGGTTTC	CAAGTGCCTGCTCCGAGAA

Table 4 *In vivo* toxicity analysis of prepared nanocomposite in Zebrafish (*Danio rerio*) embryos

In vivo property	After incubation of 48 h		After incubation of 72 h	
	Control	TG–400	Control	TG–400
Hatched (n/ab)	0/0	2/1	10/0	10/0
Unhatched (n/ab)	10/0	7/0	-	-
Dead	0	0	0	0

- n – Normal Zebrafish embryo
- ab– abnormal Zebrafish embryo

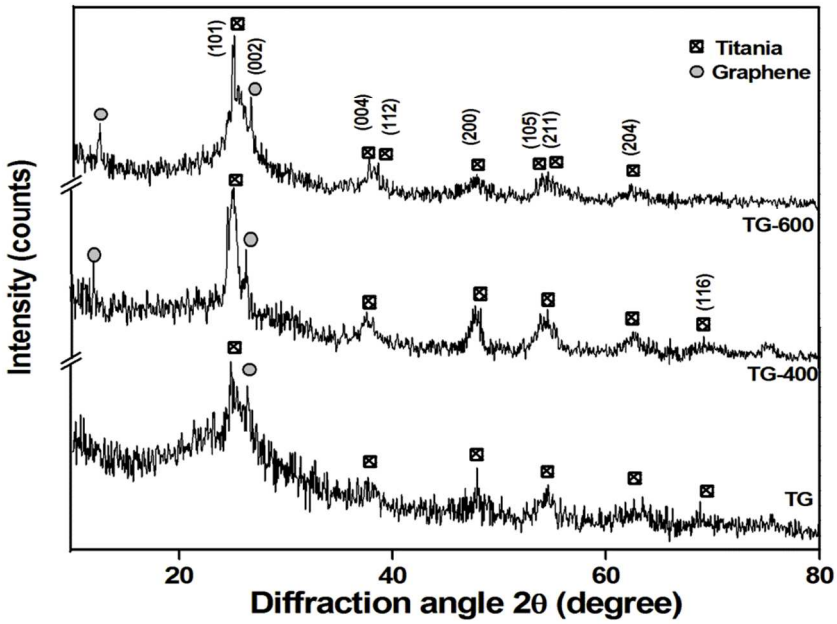

a) Before *in vitro* bioactivity study

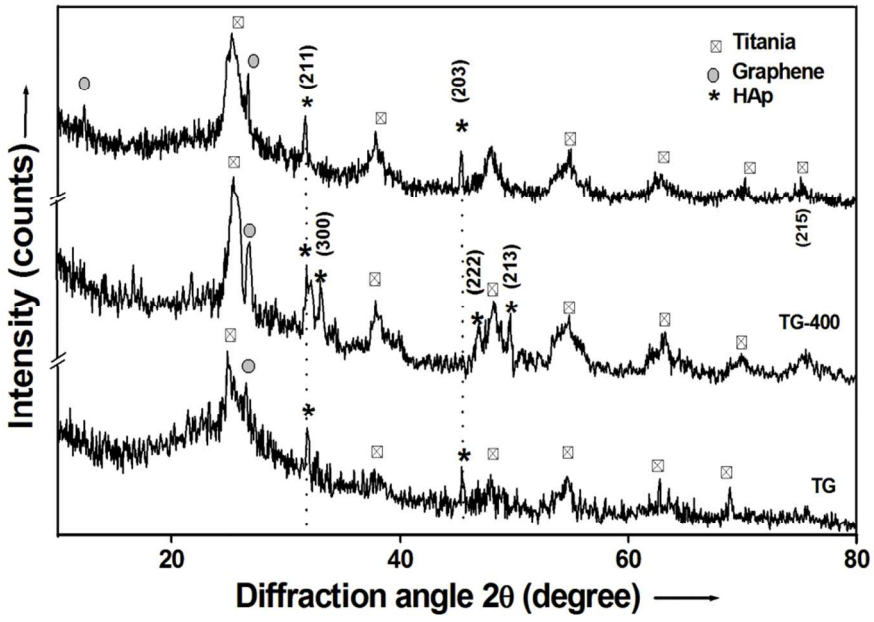

b) After *in vitro* bioactivity study

Fig. 1 X–ray diffraction pattern of a series of titania–graphene nanocomposite for bioactivity a) Before *in vitro* bioactivity and b) After *in vitro* bioactivity study

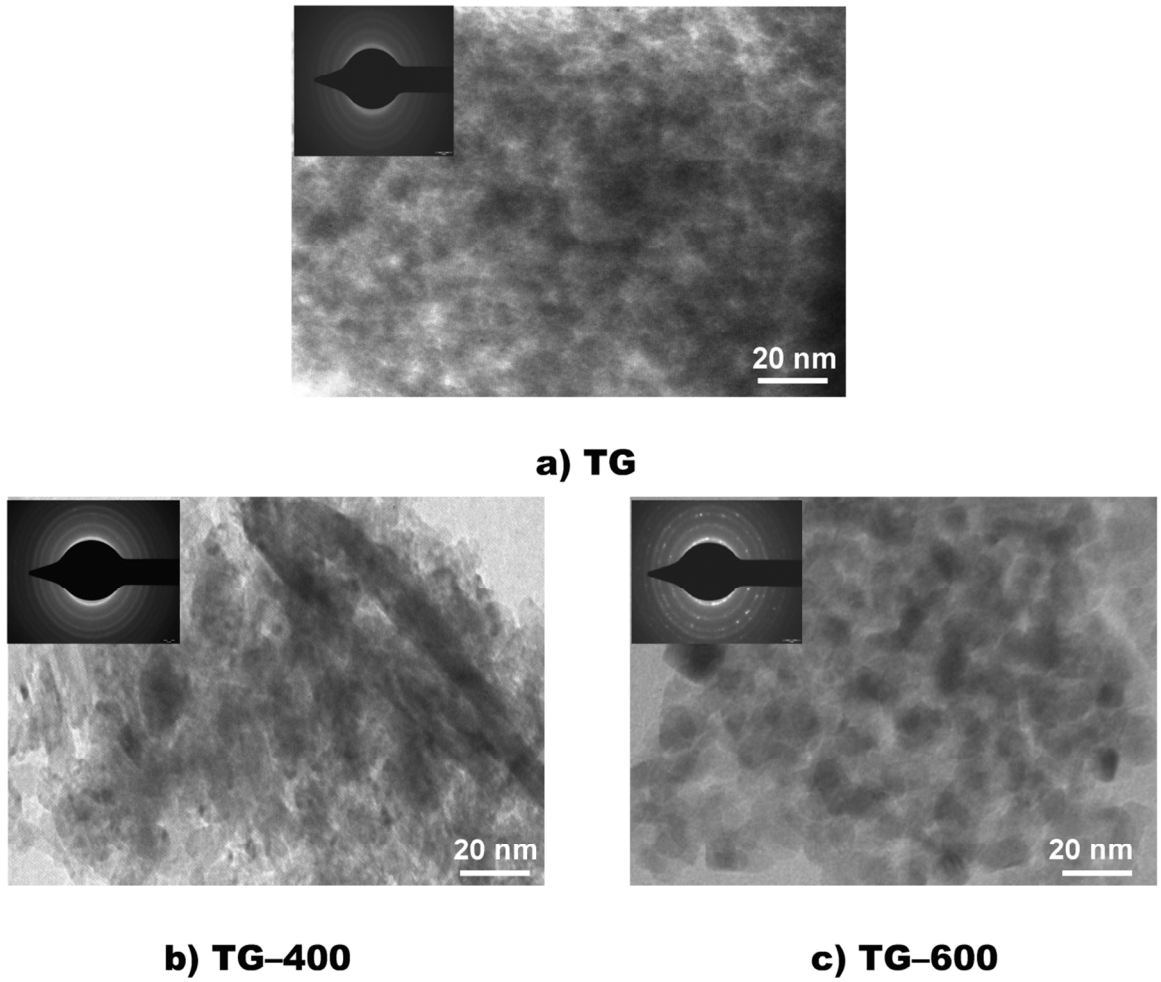

Fig. 2 Transmission electron microscopic images and corresponding diffraction pattern of prepared titania–graphene nanocomposites a) TG, b) TG-400 and c) TG-600

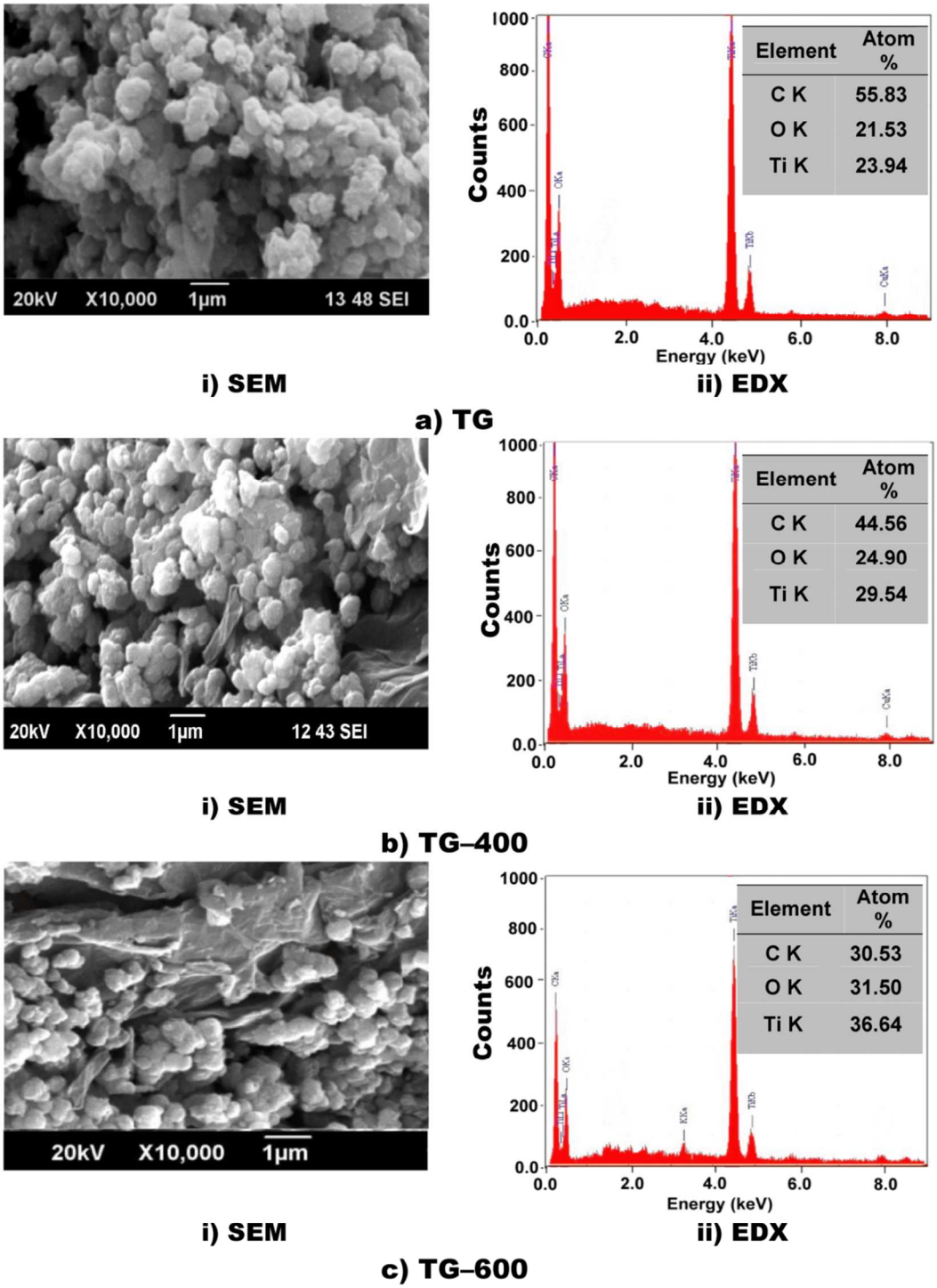

Fig. 3 Scanning electron microscopic images with respective EDX pattern of titania–graphene a) TG, b) TG-400 and c) TG-600

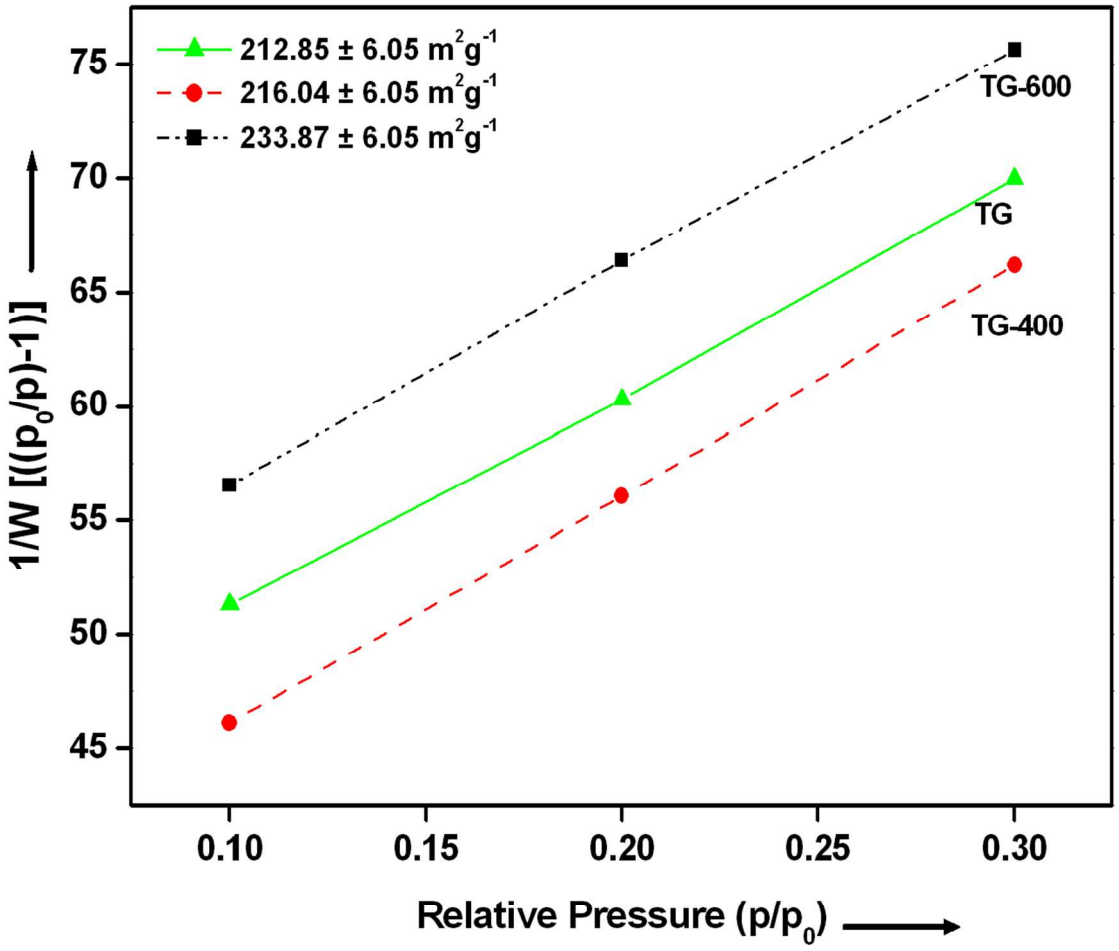

Fig. 4 BET surface area of titania–graphene composites

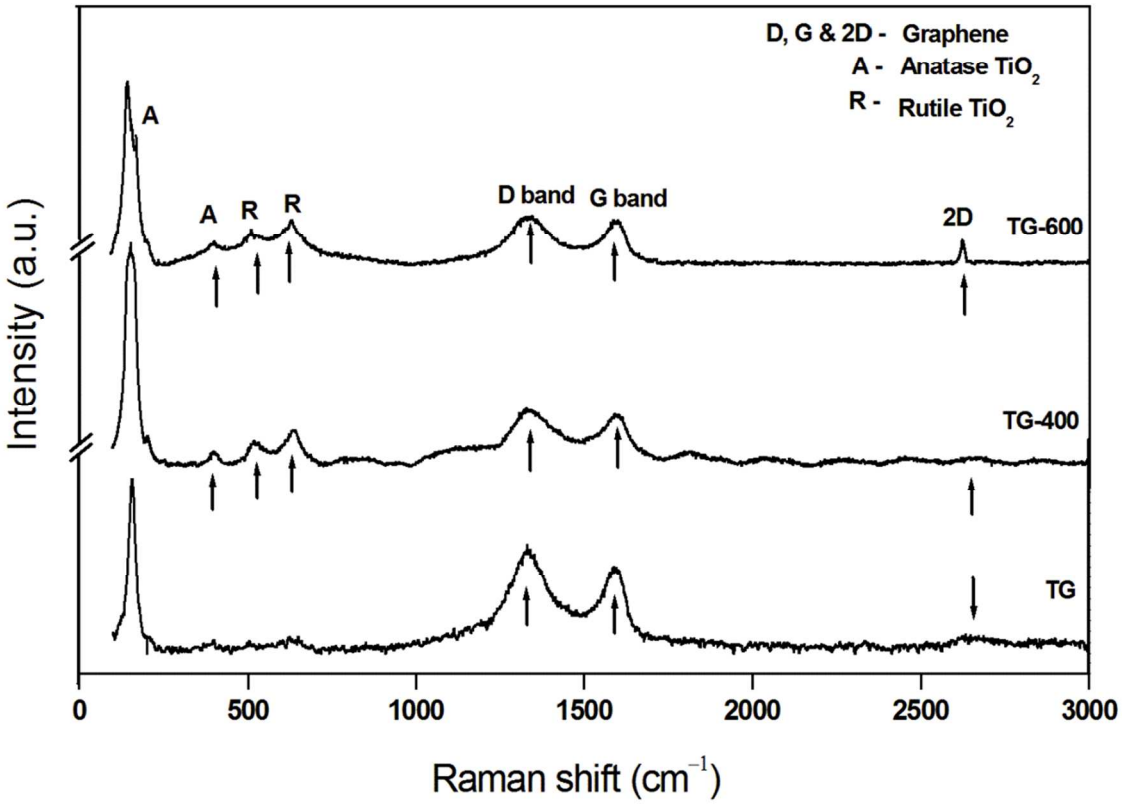

Fig. 5 Raman spectra of titania–graphene composites

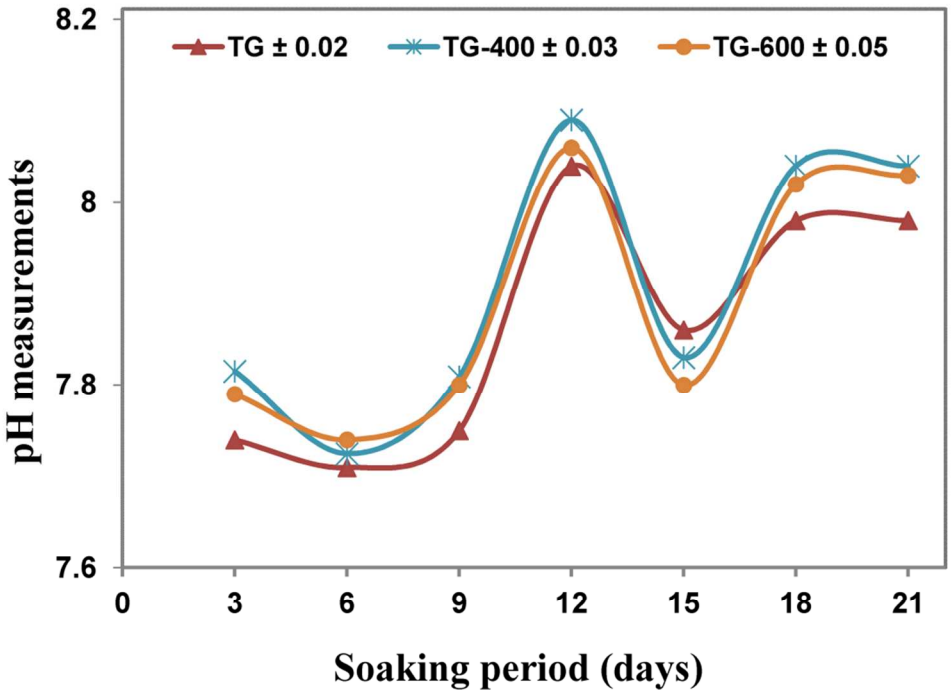

a) pH versus soaking period

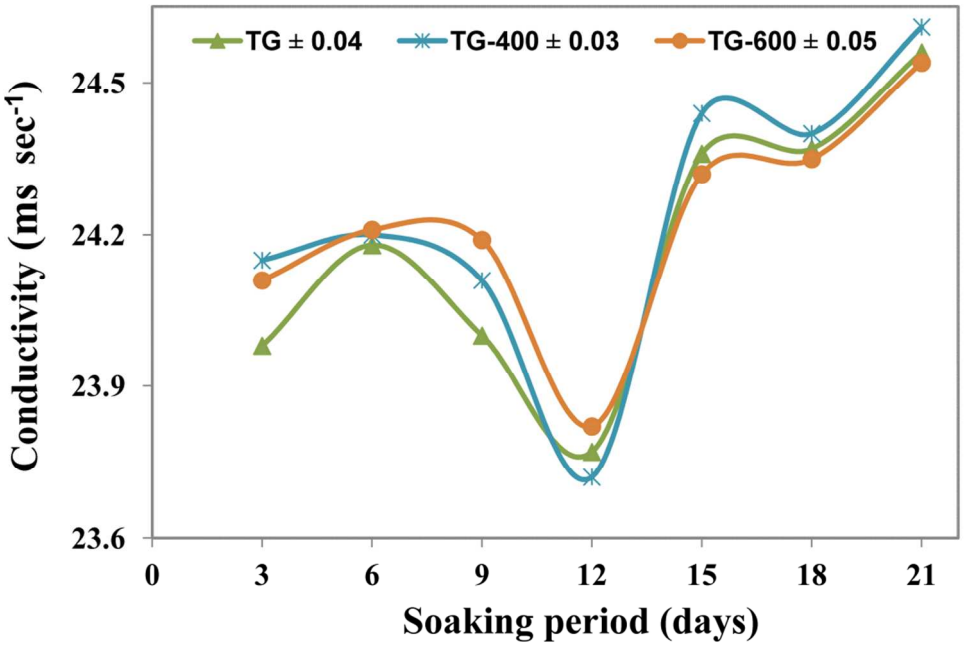

b) Conductivity during i*n vitro* bioactivity

Fig. 6 Measurmements of ionic exchanges between 1.5 SBF and titania–graphene nanocomposites a) pH versus soaking period b) Conductivity during i*n vitro* bioactivity

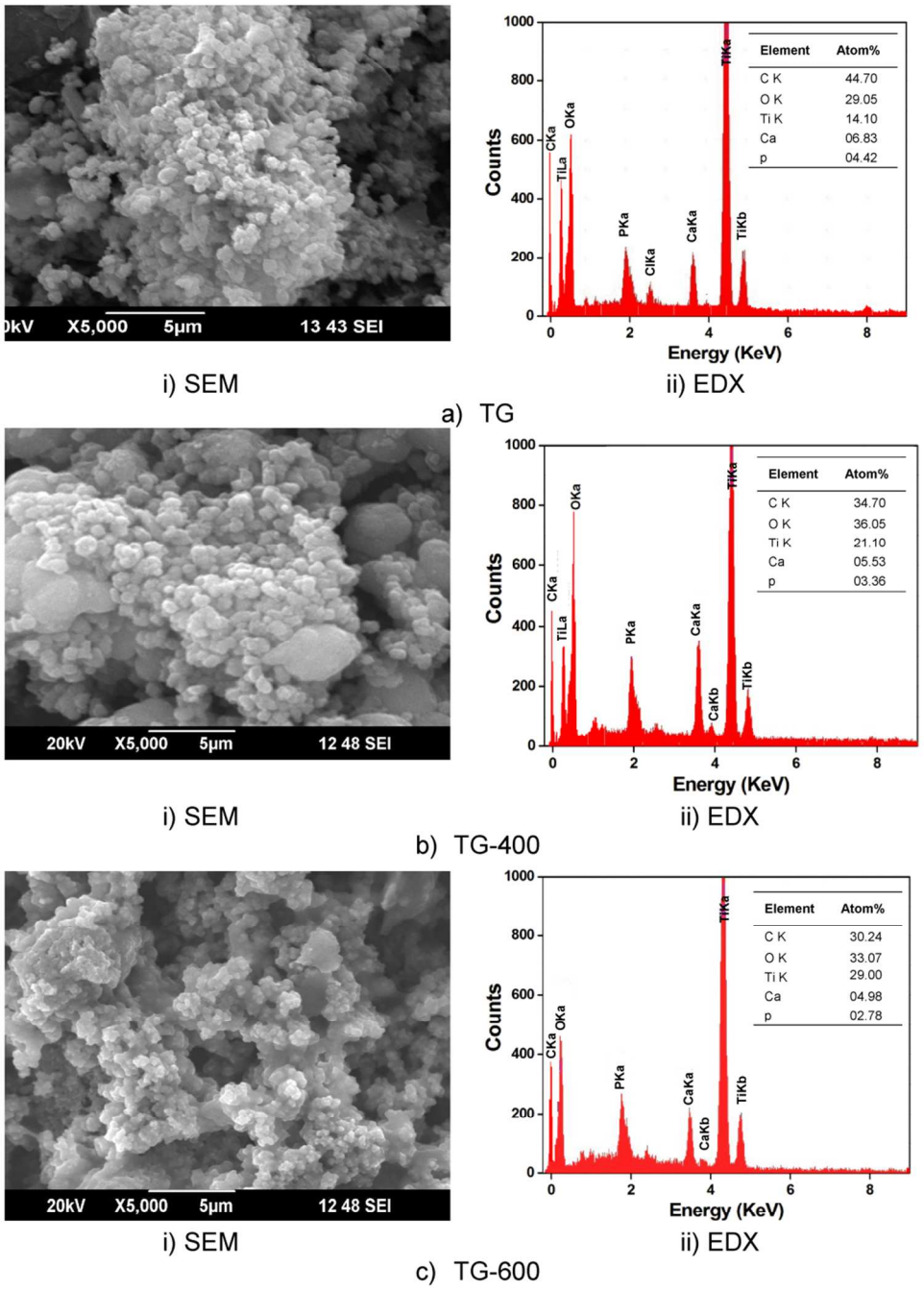

Fig. 7 SEM images with respective EDX pattern of titania–graphene after SBF bioactivity study a) TG, b) TG-400 and c) TG-600

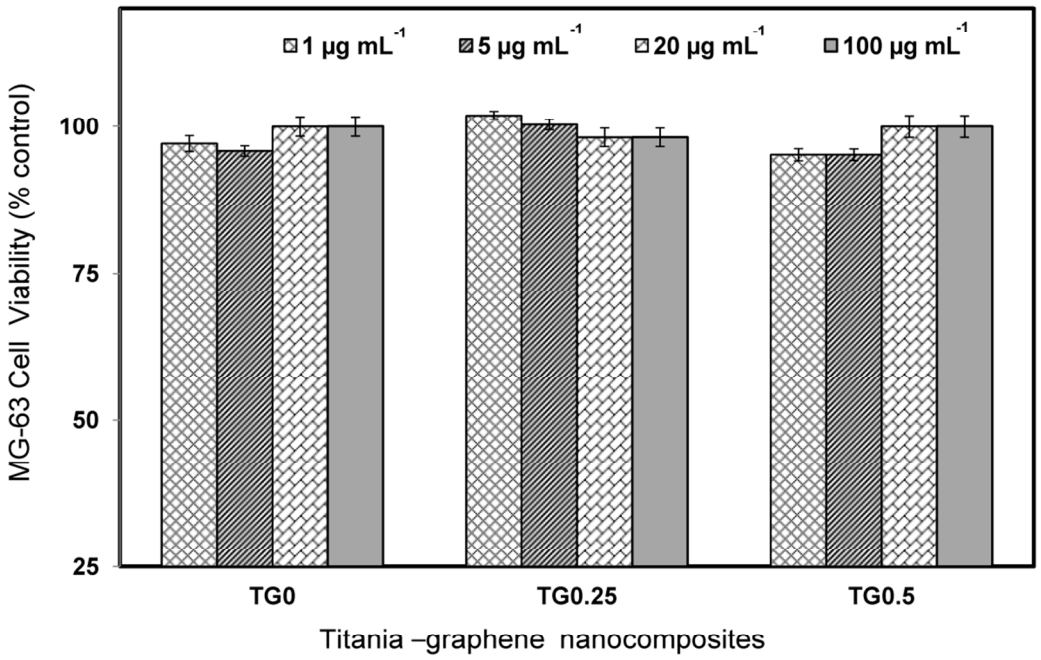

Fig. 8 Dose dependent viability of MG–63 cells incubated with different concentrations of prepared titania–graphene nanocomposites using MTT assay

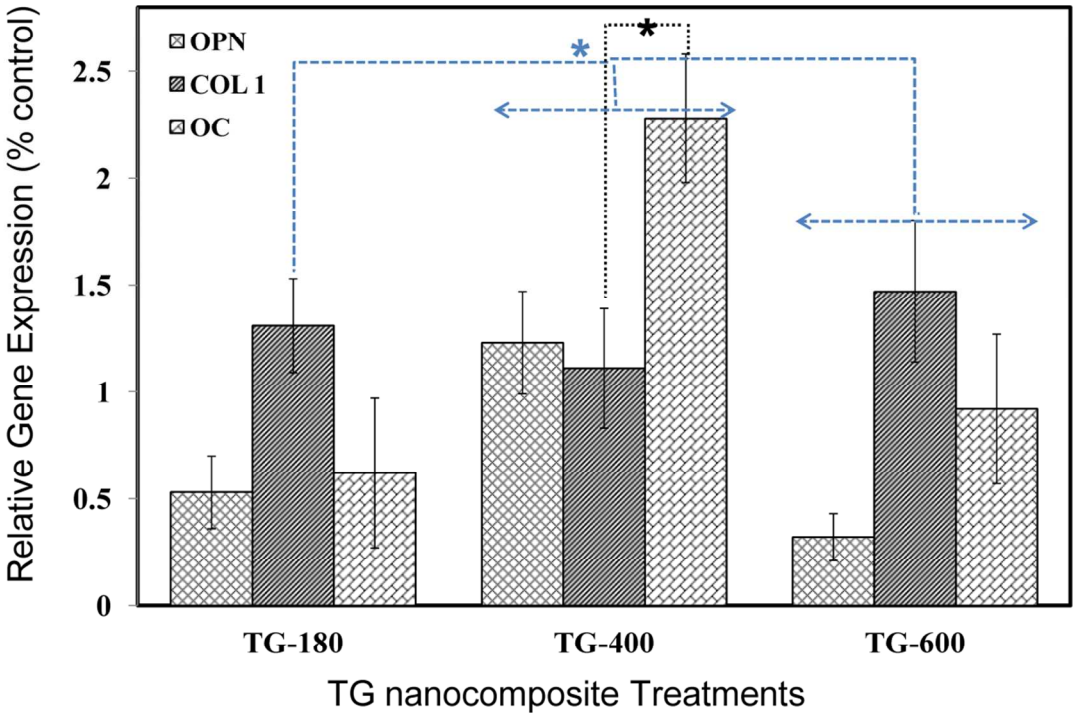

Fig. 9 Gene expression studies of TG nanocomposite treated MG–63 cell line. (*) represents significant difference at $p < 0.05$

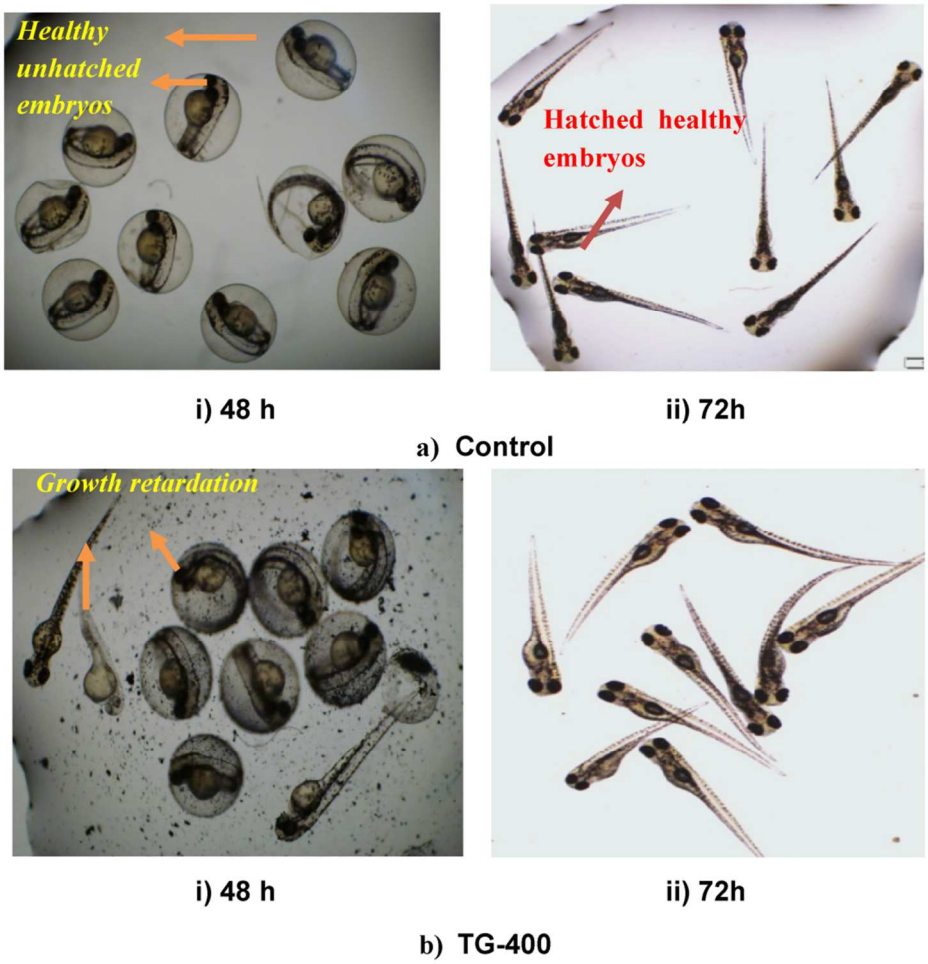

Fig. 10 Preliminary *in vivo* analysis of titania–graphene nanocomposite in zebrafish a) control and b) TG-400